Sparse-Coded Time-Delay DMD with Control for Nonlinear State-Space Modeling on Graphs

Ryuto Ito*, Hiromu Kanauchi*, Hiroyasu Yasuda*, Masaaki Nagahara† and Shogo Muramatsu*
* Niigata University, Niigata, Japan
E-mail: itory0214@gmail.com; kurou1315@gmail.com; hiro@gs.niigata-u.ac.jp; shogo@eng.niigata-u.ac.jp
† Hiroshima University, Hiroshima, Japan
E-mail: nagahara@ieee.org

***Abstract*—This study proposes a method for modeling river water-level distribution by integrating dynamic mode decomposition with control (DMDc), time-delay embedding, and sparse modeling using a graph filter bank. In a previous study, sparse-coded time-delay graph dynamic mode decomposition (STG-DMD) was proposed as a data-driven approach to derive the temporal evolution equation of water-level variations on a graph. This method achieved high reconstruction and prediction performance by incorporating the spatial connectivity among multiple points. However, because STG-DMD is formulated for autonomous systems, it has limitations in representing external inputs such as rainfall, dam discharge, and water diversion, which can significantly affect river water levels. Therefore, this study incorporates DMDc into the STG-DMD framework to derive a temporal evolution equation that explicitly accounts for control inputs while maintaining the advantages of sparse representation and the ability to capture spatial relationships through graph structures. To evaluate the effectiveness of the proposed method, time-series data generated by a process-driven model—specifically, a tank model—were used to compare the reconstruction performance across four methods: DMDc, time-delay DMDc (tdDMDc), STG-DMD, and the proposed method. The experimental results demonstrate that the proposed method achieved better reconstruction performance in most cases compared with DMDc, tdDMDc, and STG-DMD.**

I. Introduction

Severe floods have become increasingly frequent worldwide [1], [2]. In Japan, events such as Typhoon Hagibis in 2019 and other recent downpours have exposed the limits of conventional flood control. In response, the Ministry of Land, Infrastructure, Transport and Tourism launched the "River Basin Disaster Resilience and Sustainability by All" initiative in 2020[1], promoting integrated flood management through regulation, drainage, and diversion.

In parallel, hydrological modeling has advanced, particularly through system identification for extreme events. Singh *et al.* [3] showed that in single-channel systems, nonlinear runoff dynamics can be approximated linearly with water-level errors within $\pm 10\%$. In contrast, David *et al.* [4] demonstrated that in large river networks, small local errors can accumulate and interact through the network, amplifying downstream prediction errors to several tens of percent. These findings underscore the need for models that account for both spatial structure and nonlinearity.

[1]River Basin Disaster Resilience and Sustainability by All. Available at: https://www.mlit.go.jp/river/kokusai/pdf/pdf21.pdf

To address this, data-driven approaches that exploit river network structures have gained attention. Graph signal processing (GSP) has emerged as a promising framework for modeling data on irregular domains such as river basins [5]. By representing observation points as graph nodes, GSP enables the extraction of spatial patterns using a graph filter bank (GFB) [6], [7] and spectral priors [8]. These techniques have proven effective in areas such as image processing and spatiotemporal signal modeling [9], [10]. Recent work has also explored their integration with dynamical system modeling. For example, Arai *et al.* [11] incorporated graph-based sparse representation into dynamic mode decomposition (DMD) [12] for modeling river-related data. DMD-based formulations yield explicit system matrices suited for control-oriented analysis, and combined with GSP enable modeling of spatiotemporal dynamics on irregular domains.

Building on this foundation, we proposed sparse-coded time-delay graph DMD (STG-DMD) [13], [14], which enhances modeling capacity via time-delay embedding [15]. In this framework, GFB is used to extract sparse spatial features, while time-delay embedding enables high-accuracy linear approximation of nonlinear temporal dynamics. STG-DMD formulates time-evolution equations on graph structures and has shown strong performance in multipoint river water-level reconstruction and prediction. However, it assumes an autonomous system and does not explicitly incorporate external inputs such as rainfall, dam discharge, or water diversion into retention basins, which are critical for modeling non-autonomous river water-level dynamics.

To overcome this limitation, we propose STG-DMDc, an extension of STG-DMD that incorporates control inputs based on the concept of DMD with control (DMDc) [16]. This method preserves the benefits of graph-based sparse modeling and time-delay embedding while extending the framework to non-autonomous systems influenced by external inputs.

We validated STG-DMDc through numerical experiments using artificial time-series data generated by a process-driven tank model simulating river water levels. We compared its performance against DMDc, time-delay DMDc (tdDMDc) [17], [18], and the original STG-DMD. STG-DMDc achieved superior reconstruction accuracy in most cases.

The remainder of this paper is organized as follows. Section II reviews related methods and their limitations. Section III introduces the proposed STG-DMDc framework. Section IV

979-8-3315-7206-8/25/$31.00

TABLE I: Comparison of methods and their key features

Method	Graph Structure	Time Delay	Control Input
DMDc	✗	✗	✓
tdDMDc	✗	✓	✓
STG-DMD	✓	✓	✗
STG-DMDc	✓	✓	✓

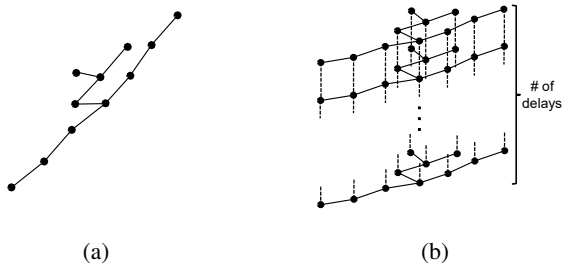

(a) (b)

Fig. 1: Overlapping graph structures in STG-DMD. (a) Original graph structure. (b) Overlapping graph structure. Solid lines represent original edges; dotted lines represent newly added edges. ©2024 IEEE. Reprinted, with permission, from [13].

describes the experimental setup and presents comparative results. Section V concludes the paper and outlines future research directions.

The main contributions of this paper are twofold.

- STG-DMDc, an extension of STG-DMD, incorporates control inputs via DMDc, enabling the modeling of non-autonomous systems influenced by external inputs.
- STG-DMDc unifies graph-based sparse representation, time-delay embedding, and dynamical system modeling with control inputs in a single data-driven framework equipped with the key characteristics summarized in Table I.

II. Review of STG-DMD and tdDMDc

This section reviews the conventional STG-DMD and td-DMDc proposed in [13], [14], [17], [18], and summarizes their issues.

A. STG-DMD

STG-DMD integrates tdDMD [19], [20] with a GFB to derive time-evolution equations for water level variations on an undirected graph $\mathcal{G}$, assuming a linear time-invariant system. tdDMD decomposes temporally varying feature vectors into spatiotemporal modes, while GFB extracts features from vertex signals on $\mathcal{G}$. STG-DMD maps the state space $\mathcal{M} \subseteq \mathbb{R}^M$ to a feature space $\tilde{\mathcal{F}} \subseteq \mathbb{R}^L$ via sparse approximation, where $M \leq L$.

The procedure is as follows. Given the graph Laplacian $\mathbf{L}$ and synthesis GFB $\mathbf{G} \in \mathbb{R}^{Md \times L}$, where d is the number of delays in the time-delay embedding:

- Prepare training data $\{\mathbf{x}_k\}_{k=0}^{N-1} \subset \mathcal{M}$.
- Apply time-delay embedding to $\mathbf{x}_k$ to form the Hankel matrix $\mathbf{X} \in \mathbb{R}^{Md \times (N-d)}$:

$$\mathbf{X} := \begin{bmatrix} \mathbf{x}_0 & \mathbf{x}_1 & \cdots & \mathbf{x}_{(N-1)-d} \\ \mathbf{x}_1 & \mathbf{x}_2 & \cdots & \mathbf{x}_{(N-1)-d+1} \\ \vdots & \vdots & \ddots & \vdots \\ \mathbf{x}_{d-1} & \mathbf{x}_d & \cdots & \mathbf{x}_{N-2} \end{bmatrix} = \begin{bmatrix} | & | & & | \\ \mathbf{h}_{\mathrm{x},0} & \mathbf{h}_{\mathrm{x},1} & \cdots & \mathbf{h}_{\mathrm{x},(N-1)-d} \\ | & | & & | \end{bmatrix}. \quad (1)$$

- Extend the graph as in Fig. 1, stacking d delays and adding edges between corresponding observation nodes.
- Map $\{\mathbf{h}_{\mathrm{x},k}\}_{k=0}^{(N-1)-d}$ to sparse-coded $\{\mathbf{y}_k\}_{k=0}^{(N-1)-d} \subset \tilde{\mathcal{F}}$ using sparse coding $\mathbf{\Psi}(\cdot)$.
- In $\tilde{\mathcal{F}}$, estimate a linear operator $\mathbf{K}$ such that $\mathbf{y}_k \simeq \mathbf{K}\mathbf{y}_{k-1}$.
- Apply DMD [12] to obtain dynamic modes $\mathbf{\Phi}$ and eigenvalues $\mathbf{\Lambda}$.

The time evolution of water levels is expressed as:

$$\mathbf{x}_k = \mathbf{P}\mathbf{G}\mathbf{\Phi}\mathbf{\Lambda}^k\mathbf{b}_0, \quad (2)$$

where $\mathbf{P} \in \mathbb{R}^{M \times Md}$ is a projection matrix, and $\mathbf{b}_0 = \mathbf{\Phi}^\dagger \mathbf{y}_0$ with $\dagger$ denoting the Moore-Penrose pseudoinverse.

Given $\mathbf{G}$, the sparse coding $\mathbf{\Psi}(\cdot)$ is defined as:

$$\mathbf{\Psi}(\mathbf{x}) := \arg\min_{\mathbf{y} \in \mathbb{R}^L} \frac{1}{2}\|\mathbf{x} - \mathbf{G}\mathbf{y}\|_2^2 + \alpha\rho(\mathbf{y}), \quad (3)$$

where $\alpha \in [0, \infty)$ is a regularization parameter. For $\rho(\cdot) = \|\cdot\|_1$, ISTA [21] updates $\mathbf{y}^{(i)}$ from $\mathbf{y}^{(0)}$ as:

$$\mathbf{y}^{(i+1)} \leftarrow \mathcal{T}_{\gamma\alpha}\left(\mathbf{y}^{(i)} - \gamma\mathbf{G}^\mathsf{T}(\mathbf{G}\mathbf{y}^{(i)} - \mathbf{x})\right), \quad i \leftarrow i+1,$$

where $\mathbf{G}^\mathsf{T}$ is the adjoint of $\mathbf{G}$ and $\mathcal{T}_{\gamma\alpha}(\cdot)$ is the soft-thresholding operator with step size γ.

It should be noted that STG-DMD is designed for autonomous systems. Therefore, it has limitations in modeling non-autonomous river water-level dynamics arising from external inputs.

B. tdDMDc

tdDMDc is a data-driven framework that combines time-delay embedding [15], [19], [20] with DMDc [16], enabling analysis of temporal evolution under both autonomous dynamics and external control inputs and allowing quantitative evaluation of control effects.

Let $\{\mathbf{x}_k\}_{k=0}^{N-1} \subset \mathcal{M} \subseteq \mathbb{R}^M$ be observed time-series data over N steps, and $\{\mathbf{u}_k\}_{k=0}^{N-1} \subset \mathbb{R}^K$ the corresponding control inputs. We denote by $\mathbf{X}$ the delay-embedded Hankel matrix constructed from $\mathbf{x}_k$, as previously defined in (1). Applying the same embedding procedure to the control inputs yields matrix $\mathbf{\Upsilon} \in \mathbb{R}^{Kd \times (N-d)}$ defined as:

$$\mathbf{\Upsilon} := \begin{bmatrix} \mathbf{u}_0 & \mathbf{u}_1 & \cdots & \mathbf{u}_{(N-1)-d} \\ \mathbf{u}_1 & \mathbf{u}_2 & \cdots & \mathbf{u}_{(N-1)-d+1} \\ \vdots & \vdots & \ddots & \vdots \\ \mathbf{u}_{d-1} & \mathbf{u}_d & \cdots & \mathbf{u}_{N-2} \end{bmatrix} = \begin{bmatrix} | & | & & | \\ \mathbf{h}_{\mathrm{u},0} & \mathbf{h}_{\mathrm{u},1} & \cdots & \mathbf{h}_{\mathrm{u},(N-1)-d} \\ | & | & & | \end{bmatrix}. \quad (4)$$

DMDc models the system evolution as:

$$\mathbf{X}_{1:N-1-d} \approx \mathbf{A}\mathbf{X}_{0:N-2-d} + \mathbf{B}\boldsymbol{\Upsilon}_{0:N-2-d}, \tag{5}$$

with $\mathbf{A} \in \mathbb{R}^{Md\times Md}$ and $\mathbf{B} \in \mathbb{R}^{Md\times Kd}$ being system and input matrices, respectively. This can be rewritten as:

$$\mathbf{X}_{1:N-1-d} \approx \begin{bmatrix}\mathbf{A} & \mathbf{B}\end{bmatrix} \begin{bmatrix}\mathbf{X}_{0:N-2-d} \\ \boldsymbol{\Upsilon}_{0:N-2-d}\end{bmatrix} = \mathbf{Q}\boldsymbol{\Omega}, \tag{6}$$

where $\mathbf{Q} := \begin{bmatrix}\mathbf{A} & \mathbf{B}\end{bmatrix}$ and $\boldsymbol{\Omega}$ is the concatenated matrix.

If $\mathbf{B}$ is unknown, estimate $\mathbf{A}$ and $\mathbf{B}$ via:

- Compute truncated SVD:

$$\boldsymbol{\Omega} \approx \tilde{\mathbf{U}}\tilde{\boldsymbol{\Sigma}}\tilde{\mathbf{V}}^*, \quad \mathbf{X}_{1:N-1-d} \approx \hat{\mathbf{U}}\hat{\boldsymbol{\Sigma}}\hat{\mathbf{V}}^*.$$

- Partition $\tilde{\mathbf{U}}$ into $\tilde{\mathbf{U}}_1 \in \mathbb{C}^{Md\times p}$ and $\tilde{\mathbf{U}}_2 \in \mathbb{C}^{Kd\times p}$.
- Estimate:

$$\tilde{\mathbf{A}} = \hat{\mathbf{U}}^*\mathbf{X}_{1:N-1-d}\tilde{\mathbf{V}}\tilde{\boldsymbol{\Sigma}}^{-1}\tilde{\mathbf{U}}_1^*\hat{\mathbf{U}}, \tag{7}$$

$$\tilde{\mathbf{B}} = \hat{\mathbf{U}}^*\mathbf{X}_{1:N-1-d}\tilde{\mathbf{V}}\tilde{\boldsymbol{\Sigma}}^{-1}\tilde{\mathbf{U}}_2^*. \tag{8}$$

- Perform eigendecomposition of $\tilde{\mathbf{A}}$ and compute dynamic modes:

$$\tilde{\mathbf{A}}\mathbf{W} = \mathbf{W}\boldsymbol{\Lambda}, \quad \boldsymbol{\Phi} = \mathbf{X}_{1:N-1-d}\tilde{\mathbf{V}}\tilde{\boldsymbol{\Sigma}}^{-1}\tilde{\mathbf{U}}_1^*\hat{\mathbf{U}}\mathbf{W}.$$

The system evolution is expressed as:

$$\mathbf{h}_{\mathrm{x},k} = \mathbf{A}\mathbf{h}_{\mathrm{x},k-1} + \mathbf{B}\mathbf{h}_{\mathrm{u},k-1}, \quad \text{where } \mathbf{A} = \boldsymbol{\Phi}\boldsymbol{\Lambda}\boldsymbol{\Phi}^\dagger. \tag{9}$$

By recursively expanding this relation, the following expression is obtained:

$$\mathbf{h}_{\mathrm{x},k} = \boldsymbol{\Phi}\boldsymbol{\Lambda}^k\boldsymbol{\Phi}^\dagger\mathbf{h}_{\mathrm{x},0} + \boldsymbol{\Phi}\sum_{i=0}^{k-1}\boldsymbol{\Lambda}^{k-i-1}\boldsymbol{\Phi}^\dagger\mathbf{B}\mathbf{h}_{\mathrm{u},i}. \tag{10}$$

While tdDMDc incorporates time-delay embedding and control inputs, it does not explicitly exploit the spatial structure of the system, potentially limiting its ability to capture spatial dependencies essential for structured spatiotemporal modeling.

III. STG-DMD with Control

This section proposes STG-DMDc, a novel extension of the conventional STG-DMD framework that incorporates external control inputs via DMDc. This extension is motivated by the limitations of STG-DMD in modeling non-autonomous systems, such as river water level dynamics influenced by external inputs. By integrating the DMDc formulation into the STG-DMD framework, STG-DMDc enables a linear approximation of nonlinear dynamical systems subject to control inputs, thus extending the framework to non-autonomous settings.

The overall procedure of STG-DMDc is illustrated in Fig. 2 and can be summarized as follows:

- Prepare time-series measurements $\{\mathbf{x}_k\}_{k=0}^{N-1} \subset \mathcal{M} \subseteq \mathbb{R}^M$ and the corresponding control inputs $\{\mathbf{u}_k\}_{k=0}^{N-1} \subset \mathbb{R}^K$.
- Apply time-delay embedding to both sequences to form the delay-embedded state matrix $\mathbf{X} \in \mathbb{R}^{Md\times(N-d)}$ and control matrix $\boldsymbol{\Upsilon} \in \mathbb{R}^{Kd\times(N-d)}$, where d is the number of delay steps.

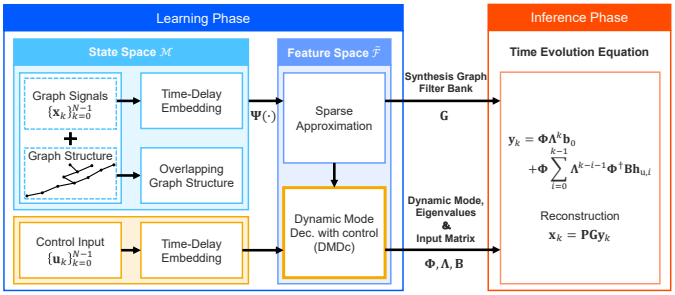

Fig. 2: Framework of STG-DMDc, where $\{\mathbf{x}_k\}_{k=0}^{N-1}$ denotes the input graph signals used for training. The nonlinear mapping $\boldsymbol{\Psi} : \mathcal{M} \to \tilde{\mathcal{F}}$ performs sparse coding, and $\mathbf{G}$ is a synthesis GFB. $\boldsymbol{\Phi}$ denotes the matrix of dynamic modes, and $\boldsymbol{\Lambda}$ is a diagonal matrix containing eigenvalues in the discrete domain. $\mathbf{P} \in \mathbb{R}^{M\times Md}$ is a projection matrix. The initial coefficient vector is defined as $\mathbf{b}_0 = \boldsymbol{\Phi}^\dagger\mathbf{y}_0$, where $\mathbf{y}_k$ is the feature vector corresponding to the k-th column of the Hankel matrix $\mathbf{X}$. The input matrix $\mathbf{B}$ models the influence of the delay-embedded control input $\mathbf{h}_{\mathrm{u},i}$.

- Extend the underlying undirected graph $\mathcal{G}$ by stacking d delayed replicas and introducing inter-layer connections between corresponding nodes across delay steps, thereby constructing an overlapping graph structure as depicted in Fig. 1.
- Map the delay-embedded state vectors $\{\mathbf{h}_{\mathrm{x},k}\}_{k=0}^{(N-1)-d}$ into a high-dimensional feature space $\tilde{\mathcal{F}}$ via sparse coding using function $\boldsymbol{\Psi}(\cdot)$, which is defined with respect to the synthesis GFB $\mathbf{G}$. This yields the sparse-coded feature vectors $\{\mathbf{y}_k\}_{k=0}^{(N-1)-d}$. We denote by $\mathbf{Y} \in \mathbb{R}^{L\times(N-d)}$ the matrix formed by stacking these feature vectors:

$$\mathbf{Y} = \begin{bmatrix}\mathbf{y}_0 & \mathbf{y}_1 & \cdots & \mathbf{y}_{(N-1)-d}\end{bmatrix}.$$

- Apply DMDc to the feature-domain sequences to jointly model the evolution of the system states and the effects of control inputs. The system dynamics are approximated as:

$$\mathbf{Y}_{1:N-1-d} \approx \mathbf{A}\mathbf{Y}_{0:N-2-d} + \mathbf{B}\boldsymbol{\Upsilon}_{0:N-2-d}. \tag{11}$$

- Estimate the system matrix $\mathbf{A}$ and input matrix $\mathbf{B}$ using truncated SVD, as described in Section II-B.
- Perform eigendecomposition of $\mathbf{A}$ to obtain the eigenvalues $\boldsymbol{\Lambda}$ and eigenvectors $\mathbf{W}$, and compute the dynamic modes in the feature space as:

$$\boldsymbol{\Phi} = \mathbf{Y}_{1:N-1-d}\tilde{\mathbf{V}}\tilde{\boldsymbol{\Sigma}}^{-1}\tilde{\mathbf{U}}_1^*\hat{\mathbf{U}}\mathbf{W}. \tag{12}$$

The temporal evolution of the feature vector $\mathbf{y}_k$ is given by:

$$\mathbf{y}_k = \boldsymbol{\Phi}\boldsymbol{\Lambda}^k\mathbf{b}_0 + \boldsymbol{\Phi}\sum_{i=0}^{k-1}\boldsymbol{\Lambda}^{k-i-1}\boldsymbol{\Phi}^\dagger\mathbf{B}\mathbf{h}_{\mathrm{u},i}. \tag{13}$$

The corresponding water level at time step k is reconstructed from the feature space using the synthesis GFB $\mathbf{G} \in \mathbb{R}^{Md\times L}$ and a projection matrix $\mathbf{P} \in \mathbb{R}^{M\times Md}$:

$$\mathbf{x}_k = \mathbf{P}\mathbf{G}\mathbf{y}_k. \tag{14}$$

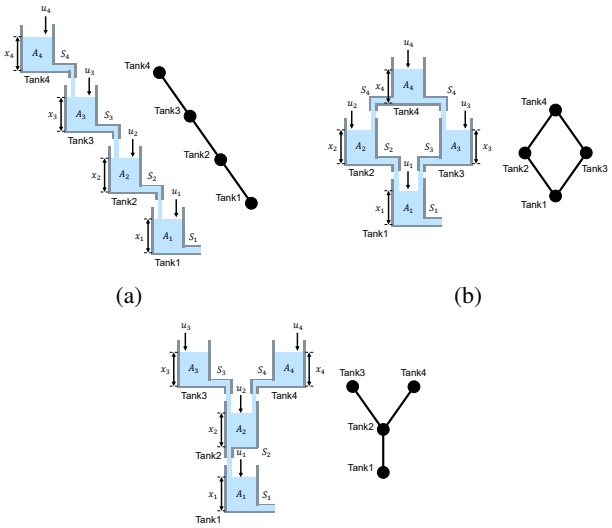

Fig. 3: Schematic diagrams of (a) series, (b) parallel, and (c) merged tank models. In each, x_i, A_i, S_i, and u_i denote water level, tank area, outlet area, and control input. Right-side graphs illustrate the corresponding graph structures.

TABLE II: Tank model parameters and control inputs $u_{i,k}$ for each tank i at time step k used during the inference phase.

Common parameters	
Initial water level $x_{0,i}$ [m]	15
Tank area A_i [m^2]	1000
Outlet area S_i [m^2]	1
Gravity g [m/s^2]	9.81
Simulation duration T [s]	5000
Control inputs $u_{i,k}$ [m^3/s]	
Tank 1	$\begin{cases} 1.0 & 1000 \le k \le 2000 \\ 0 & \text{otherwise} \end{cases}$
Tank 2	$\begin{cases} 3.0 & 1500 \le k \le 2000 \\ 1.0 & 2501 \le k \le 3000 \\ -1.0 & 3001 \le k \le 3500 \\ 0 & \text{otherwise} \end{cases}$
Tank 3	$\begin{cases} 1.5\left(1+\sin\left(\frac{2\pi(k-20)}{1000}\right)\right) & 750 \le k \le 2750 \\ 0 & \text{otherwise} \end{cases}$
Tank 4	$\begin{cases} 7.0 & 250 \le k \le 1000 \\ 0 & \text{otherwise} \end{cases}$

IV. Performance Evaluation

This section presents a performance evaluation of the proposed STG-DMDc framework using artificial data.

A. Artificial Data Experiment

To assess the reconstruction performance of the proposed method, artificial time-series data of water-level distributions were generated using a process-driven tank model. This model simulates fluid flow among interconnected tanks based on fundamental hydraulic principles. We constructed time-evolution equations using several data-driven approaches and compared the reconstructed water-level profiles with those derived from the original nonlinear state equations.

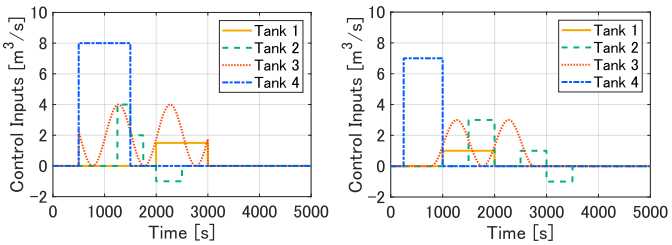

(a) Learning-phase inputs (b) Inference-phase inputs

Fig. 4: Time-series of control inputs $u_{i,k}$ for Tanks 1–4.

TABLE III: GFB design parameters for the proposed method

Tank model	Series	Parallel	Merged
Filter type	Half cosine	Half cosine	Half cosine
Number of filters	8	8	8
Step size γ	8.0×10^{-1}	8.0×10^{-1}	8.0×10^{-1}
Reg. param. α	5.4×10^{-2}	2.1×10^{-2}	6.9×10^{-2}

To examine the impact of incorporating graph structures on reconstruction accuracy, we considered three distinct configurations of four interconnected tanks, each defined by a different connectivity structure:

- Series Tank Model: Four tanks connected sequentially in a linear arrangement.
- Parallel Tank Model: One upstream tank diverging into two parallel tanks, which then converge into a single downstream tank.
- Merged Tank Model: Two upstream tanks merging into an intermediate tank, followed by a final downstream tank.

Schematic diagrams of these configurations are shown in Fig. 3. The parameter values used in the experiments are summarized in Table II, representing an idealized small-scale urban catchment. To ensure consistent benchmarking, a slightly elevated hydraulic gradient and a shortened flood duration were employed across all configurations, thereby providing sufficient dynamic range for quantitative comparison with the reference nonlinear model.

The control inputs $u_{i,k}$ were heuristically designed to reflect representative hydrological scenarios: moderate constant rainfall for Tank 1, stepwise rainfall followed by a reduction in inflow, representing water diversion from the system, for Tank 2, periodic inflow due to dam release for Tank 3, and intense constant rainfall for Tank 4. Although not derived from observed data, these idealized inputs emulate commonly observed hydrological behaviors and facilitate systematic evaluation of each modeling method. Fig. 4 illustrates the control inputs for the learning and inference phases, with the latter corresponding to the settings in Table II.

The specifications of the GFB used in this study are presented in Table III. A half-cosine basis was adopted for filter design, implemented using the GSPBox[2]. The projection matrices $\mathbf{P}$, defined in (14), were set to the form $\begin{bmatrix}\mathbf{I}\ \mathbf{O}\ \cdots\ \mathbf{O}\end{bmatrix}$, where $\mathbf{I}$ is the identity matrix and $\mathbf{O}$ denotes zero matrices. The number of delays in the time-delay embedding was set to

[2]GSPBox. Available at: https://epfl-lts2.github.io/gspbox-html/

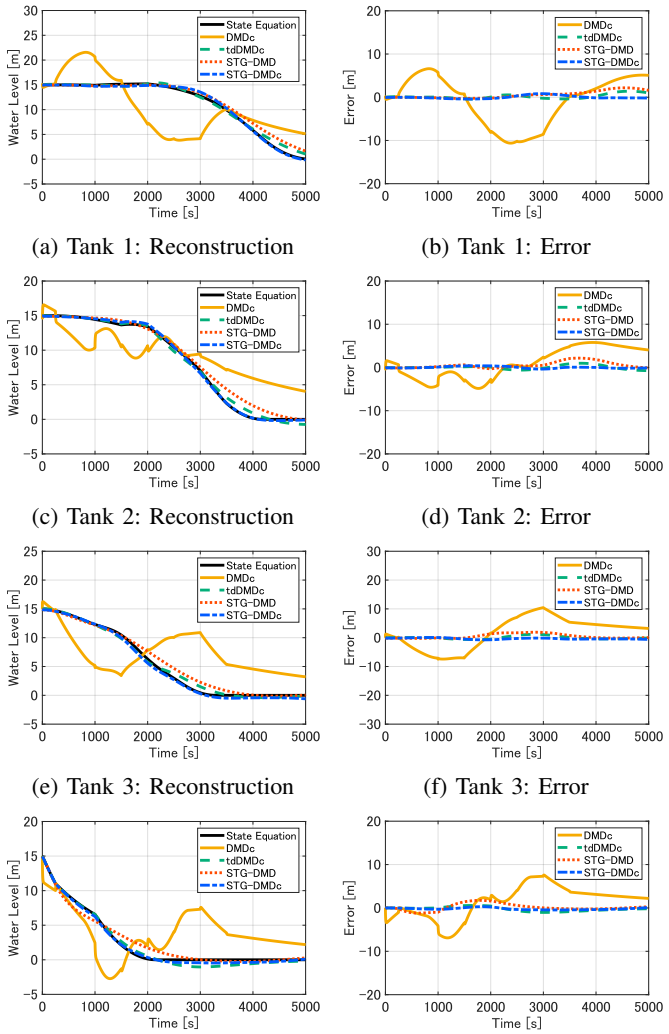

(a) Tank 1: Reconstruction (b) Tank 1: Error

(c) Tank 2: Reconstruction (d) Tank 2: Error

(e) Tank 3: Reconstruction (f) Tank 3: Error

(g) Tank 4: Reconstruction (h) Tank 4: Error

Fig. 5: Reconstruction results and corresponding errors for each tank in the series tank model.

$d = 5$ as a representative value, since we also conducted tests with $d = 7$ and 9, and these showed no noticeable differences in reconstruction performance.

B. Reconstruction Results

We evaluated the reconstruction accuracy of four approaches: DMDc, tdDMDc, STG-DMD, and the proposed STG-DMDc. These methods were applied to the three tank configurations described above.

Fig. 5 illustrates the reconstructed water levels and corresponding errors for each tank in the series configuration as a representative example. Table IV summarizes the root mean square error (RMSE) for each method and tank configuration. The results demonstrate that integrating both time-delay embedding and graph-based spatial modeling significantly enhances reconstruction accuracy. STG-DMDc achieved the lowest RMSE in most cases, validating its effectiveness in modeling complex spatiotemporal dynamics.

A comparison of the methods highlights the contribution

TABLE IV: RMSE [m] for each tank model

Tank	DMDc	tdDMDc	STG-DMD	STG-DMDc (proposed)
Series tank model				
Tank1	5.6355	0.5567	0.9810	**0.3515**
Tank2	3.6597	0.4476	0.9134	**0.2163**
Tank3	5.6926	0.5103	0.9375	**0.3997**
Tank4	3.9502	0.5508	0.8036	**0.2930**
Parallel tank model				
Tank1	6.1161	1.0895	1.3165	**0.5716**
Tank2	2.5769	0.7591	0.4886	**0.3895**
Tank3	2.5327	0.6497	0.6347	**0.3398**
Tank4	2.3193	0.7793	**0.3517**	0.4167
Merged tank model				
Tank1	6.3661	0.9905	1.1518	**0.3697**
Tank2	6.6548	0.8172	1.0386	**0.2877**
Tank3	3.8693	0.1757	0.1684	**0.1079**
Tank4	3.7689	0.3839	0.7174	**0.3658**

of each modeling component. DMDc, which lacks both time-delay embedding and spatial modeling, yields the largest errors. tdDMDc captures temporal dependencies through delay embedding but ignores spatial structure. STG-DMD leverages spatial structure through graph representation but omits control inputs. By integrating all three—temporal, spatial, and control modeling—STG-DMDc achieves the most accurate reconstructions. These results confirm that each component enhances model expressiveness, and their integration is essential for modeling nonlinear, non-autonomous systems. Notably, STG-DMDc maintained high accuracy even under strongly nonlinear conditions, such as rapid water-level drops within one hour in storage-dominated systems, suggesting its potential to exceed the limitations of linear approximation models.

V. Conclusion

This study proposed STG-DMDc, an extension of STG-DMD that incorporates control inputs via DMDc. By combining sparse coding with a GFB and time-delay embedding in the feature space, STG-DMDc models nonlinear spatiotemporal dynamics under external influences, while retaining the benefits of graph-based spatial representation.

The effectiveness of the proposed method was validated through numerical experiments using artificial data generated from a tank model. Across most evaluated configurations, STG-DMDc achieved improved reconstruction performance compared with DMDc, tdDMDc, and STG-DMD. These results demonstrate the method's potential to model river water-level dynamics under external inputs.

Future work includes extending the method to directed graphs that reflect river flow directions, validating its predictive performance with real data from rivers of different scales such as small catchments and the Shinano River, the longest river in Japan, analyzing how input conditions and graph structures affect its applicability, and exploring a trainable dictionary as a replacement for the fixed GFB.

Acknowledgments

This work was supported by JSPS KAKENHI Grant Numbers JP22H00512, JP24H00365, and JP24K21314.

References

[1] N. W. Arnell and S. N. Gosling, "The impacts of climate change on river flood risk at the global scale," *Climatic Change*, vol. 134, no. 3, pp. 387–401, 2016. DOI: 10.1007/s10584-014-1084-5.

[2] H. Alifu, Y. Hirabayashi, Y. Imada, and H. Shiogama, "Enhancement of river flooding due to global warming," *Scientific Reports*, vol. 12, p. 20 687, 2022. DOI: 10.1038/s41598-022-25182-6.

[3] V. Singh, S. Jain, and M. Sherif, "Errors of kinematic wave and diffusion wave approximations for time-independent flows with infiltration and momentum exchange included," *Hydrological Processes*, vol. 19, pp. 1771–1790, Jun. 2005. DOI: 10.1002/hyp.5633.

[4] C. H. David, J. M. Hobbs, M. J. Turmon, C. M. Emery, J. T. Reager, and J. S. Famiglietti, "Analytical propagation of runoff uncertainty into discharge uncertainty through a large river network," *Geophysical Research Letters*, vol. 46, no. 14, pp. 8102–8113, 2019. DOI: https://doi.org/10.1029/2019GL083342.

[5] A. Ortega, P. Frossard, J. Kovačević, J. M. F. Moura, and P. Vandergheynst, "Graph signal processing: Overview, challenges, and applications," *Proceedings of the IEEE*, vol. 106, no. 5, pp. 808–828, 2018. DOI: 10.1109/JPROC.2018.2820126.

[6] A. Sakiyama, K. Watanabe, Y. Tanaka, and A. Ortega, "Two-channel critically sampled graph filter banks with spectral domain sampling," *IEEE Transactions on Signal Processing*, vol. 67, no. 6, pp. 1447–1460, Mar. 2019, ISSN: 1941-0476. DOI: 10.1109/tsp.2019.2892033.

[7] E. Pavez, B. Girault, A. Ortega, and P. A. Chou, "Two channel filter banks on arbitrary graphs with positive semi definite variation operators," *IEEE Transactions on Signal Processing*, vol. 71, pp. 917–932, 2023. DOI: 10.1109/TSP.2023.3257983.

[8] S. Bagheri, T. T. Do, G. Cheung, and A. Ortega, "Spectral graph learning with core eigenvectors prior via iterative glasso and projection," *IEEE Transactions on Signal Processing*, vol. 72, pp. 3958–3972, 2024. DOI: 10.1109/TSP.2024.3446453.

[9] I. Rotondo, G. Cheung, A. Ortega, and H. E. Egilmez, "Designing sparse graphs via structure tensor for block transform coding of images," in *2015 Asia-Pacific Signal and Information Processing Association Annual Summit and Conference (APSIPA)*, 2015, pp. 571–574. DOI: 10.1109/APSIPA.2015.7415334.

[10] C. Pan, S. Chen, and A. Ortega, "Spatio-temporal graph scattering transform," in *Proc. International Conference on Learning Representations (ICLR)*, 2021.

[11] Y. Arai, S. Muramatsu, H. Yasuda, K. Hayasaka, and Y. Otake, "Sparse-coded dynamic mode decomposition on graph for prediction of river water level distribution," in *ICASSP 2021 - 2021 IEEE International Conference on Acoustics, Speech and Signal Processing (ICASSP)*, 2021, pp. 3225–3229. DOI: 10.1109/ICASSP39728.2021.9414533.

[12] J. H. Tu, C. W. Rowley, D. M. Luchtenburg, S. L. Brunton, and J. N. Kutz, "On dynamic mode decomposition: Theory and applications," *Journal of Computational Dynamics*, vol. 1, no. 2, pp. 391–421, 2014. DOI: 10.3934/jcd.2014.1.391.

[13] R. Ito, T. Naito, H. Yasuda, M. Nagahara, and S. Muramatsu, "Sparse-coded time-delay graph DMD for prediction of river water level distribution," in *2024 International Technical Conference on Circuits/Systems, Computers, and Communications (ITC-CSCC)*, 2024, pp. 1–5. DOI: 10.1109/ITC-CSCC62988.2024.10628276.

[14] R. Ito, H. Kanauchi, T. Naito, H. Yasuda, M. Nagahara, and S. Muramatsu, "Sparse-coded time-delay graph DMD for nonlinear state-space modeling on graphs," *submitted to IEICE Transactions on Fundamentals of Electronics, Communications and Computer Sciences*, 2025, Manuscript under review.

[15] S. L. Brunton, B. W. Brunton, J. L. Proctor, E. Kaiser, and J. N. Kutz, "Chaos as an intermittently forced linear system," *Nature Communications*, vol. 8, no. 1, May 2017, ISSN: 2041-1723. DOI: 10.1038/s41467-017-00030-8.

[16] J. L. Proctor, S. L. Brunton, and J. N. Kutz, "Dynamic mode decomposition with control," *SIAM Journal on Applied Dynamical Systems*, vol. 15, no. 1, pp. 142–161, 2016. DOI: 10.1137/15M1013857.

[17] S. L. Brunton, M. Budišić, E. Kaiser, and J. N. Kutz, "Modern koopman theory for dynamical systems," *SIAM Review*, vol. 64, no. 2, pp. 229–340, 2022. DOI: 10.1137/21M1401243.

[18] E. Kaiser, J. N. Kutz, and S. L. Brunton, "Sparse identification of nonlinear dynamics for model predictive control in the low-data limit," *Proceedings of the Royal Society A: Mathematical, Physical and Engineering Sciences*, vol. 474, no. 2219, p. 20 180 335, 2018. DOI: 10.1098/rspa.2018.0335.

[19] S. Pan and K. Duraisamy, "On the structure of time-delay embedding in linear models of non-linear dynamical systems," *Chaos: An Interdisciplinary Journal of Nonlinear Science*, vol. 30, no. 7, p. 073 135, Jul. 2020, ISSN: 1054-1500. DOI: 10.1063/5.0010886.

[20] D. Dylewsky, E. Kaiser, S. L. Brunton, and J. N. Kutz, "Principal component trajectories for modeling spectrally continuous dynamics as forced linear systems," *Phys. Rev. E*, vol. 105, p. 015 312, 1 Jan. 2022. DOI: 10.1103/PhysRevE.105.015312.

[21] I. Daubechies, M. Defrise, and C. Mol, "An iterative thresholding algorithm for linear inverse problems with a sparsity constraint," *Communications on Pure and Applied Mathematics*, vol. 57, Nov. 2004. DOI: 10.1002/cpa.20042.